 Related Commentary, page 16

Myeloid cell expression of the RNA-binding protein HuR protects mice from pathologic inflammation and colorectal carcinogenesis

Anthie Yiakouvaki,[1] Marios Dimitriou,[1] Ioannis Karakasiliotis,[1] Christina Eftychi,[1] Stamatis Theocharis,[2] and Dimitris L. Kontoyiannis[1]

[1]Institute of Immunology, Biomedical Sciences Research Center "Alexander Fleming," Vari, Greece.
[2]First Department of Pathology, School of Medicine, National and Kapodistrian University of Athens, Athens, Greece.

The innate immune response involves a variety of inflammatory reactions that can result in inflammatory disease and cancer if they are not resolved and instead are allowed to persist. The effective activation and resolution of innate immune responses relies on the production and posttranscriptional regulation of mRNAs encoding inflammatory effector proteins. The RNA-binding protein HuR binds to and regulates such mRNAs, but its exact role in inflammation remains unclear. Here we show that HuR maintains inflammatory homeostasis by controlling macrophage plasticity and migration. Mice lacking HuR in myeloid-lineage cells, which include many of the cells of the innate immune system, displayed enhanced sensitivity to endotoxemia, rapid progression of chemical-induced colitis, and severe susceptibility to colitis-associated cancer. The myeloid cell–specific HuR-deficient mice had an exacerbated inflammatory cytokine profile and showed enhanced CCR2-mediated macrophage chemotaxis. At the molecular level, activated macrophages from these mice showed enhancements in the use of inflammatory mRNAs (including *Tnf*, *Tgfb*, *Il10*, *Ccr2*, and *Ccl2*) due to a lack of inhibitory effects on their inducible translation and/or stability. Conversely, myeloid overexpression of HuR induced posttranscriptional silencing, reduced inflammatory profiles, and protected mice from colitis and cancer. Our results highlight the role of HuR as a homeostatic coordinator of mRNAs that encode molecules that guide innate inflammatory effects and demonstrate the potential of harnessing the effects of HuR for clinical benefit against pathologic inflammation and cancer.

Introduction

Induction, regulation, and resolution of the innate immune response involves a wide spectrum of inflammatory reactions (1, 2). Cellular damage or pathogens are initially detected by pattern recognition receptors and stress sensors on scavenging cells such as tissue and sentinel macrophages and dendritic cells. Proinflammatory cytokines, chemokines, and other small mediators then enhance vasodilation, neutrophil extravasation, and acquisition of plasma components such as complement and antibodies, to destroy pathogens and damaged cells. As inciting agents are cleared by a first line of phagocytes, inflammation changes to accommodate tissue clearance, repair, and immune homeostasis. This transition is characterized by a chemokine-dependent switch from neutrophil to monocyte recruitment, and the subsequent appearance of alternatively activated macrophages that secrete antiinflammatory, tissue remodeling, and angiogenic factors (1–3). These responses can be polarized further toward a proinflammatory (M1) state or an alternative (M2) state by the integration of adaptive immunity helper signals such as Th1/Th2 lymphokines (1, 3). The persistence of any given innate response could result in inflammatory disease and cancer. If inflammatory triggers cannot cease and be eliminated, or if the proinflammatory state persists, inflammation converts to a chronic response, which contributes to tissue damage, mutation and neoplasia, tumor growth, angiogenesis, and metastasis (4, 5).

The efficacy of the innate immune response relies on the production and posttranscriptional regulation of mRNAs encoding effector proteins (6, 7). Such labile mRNAs often contain adenylate uridylate–rich elements (AREs) in their untranslated termini and interact with RNA-binding proteins (RBPs) that may also bind to populations of small RNAs. Specific ribonucleoprotein (RNP) complexes are targeted by inflammatory signals to control the intracellular transport, translation, and decay of the inflammatory mRNAs (7–9). RBPs such as TTP, BRF1, hnRNPD/AUF1, KSRP, and TIA1/TIAR can stall translation and promote ARE-mediated mRNA decay (AMD). Mechanisms of decay may involve the exosome, proteasome, microRNAs, stress granules, and P-bodies (6, 8, 10–12). The importance of this negative, ARE-mediated control is underlined by the development of inflammatory pathologies in transgenic mice with dysfunctional AREs or ARE-binding proteins (ARE-BPs) (13).

RBPs that in turn act against AMD include members of the *Elavl/Hu* family. The prototype Elavl1/HuR is a ubiquitously expressed protein that binds to a U-rich RNA motif and shuttles between nucleus and cytoplasm via interactions with nuclear export/import adaptors. Posttranslational modifications of HuR suggest that its localization and target binding could be controlled by proliferation and stress signals (14). The RNA recognition motifs of HuR interact with mRNAs involved in cell cycle, cell death and differentiation, immunity, and inflammation. HuR has been proposed to act in cytoplasm as the stabilizer of ARE-related mRNA by enhancing the stability of some of its target mRNAs while antagonizing their binding to destabilizing RBPs or microRNAs (12, 15). Changes in HuR levels or localization in clinical samples from inflammation or cancer patients have therefore been interpreted in terms of its proinflammatory and pro-tumorigenic activities (16, 17). However, HuR can also negatively affect mRNA translation without interfering

Conflict of interest: The authors have declared that no conflict of interest exists.
Citation for this article: *J Clin Invest.* 2012;122(1):48–61. doi:10.1172/JCI45021.

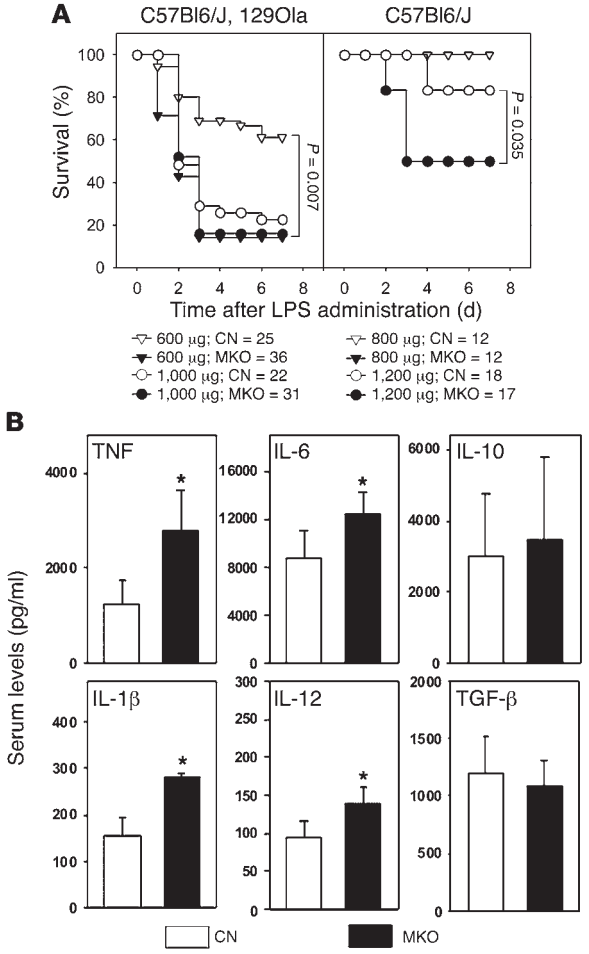

Figure 1

Myeloid deletion of HuR increases sensitivity to LPS-induced endotoxemia. (**A**) Kaplan-Meier distribution of control (CN) and MKO mice that survived endotoxemia induced by increasing doses of LPS (per 25 g of body weight). Data were collected from mice on a mixed C57BL/6J, 129Ola or inbred C57BL/6J background. Group numbers and *P* values of statistically significant differences are shown. (**B**) Cytokine levels in sera from control and MKO mice after administration of LPS (100 μg/25 g of body weight). Bar graphs depict mean values ± SEM from more than 10 mice per group. $*P \leq 0.05$.

with turnover or promoting destabilization in some of its targets, through synergies with suppressive RBPs, microRNAs, and associated factors (18–22). Overexpression of HuR in mouse macrophages blocks the translation of selective inflammatory mRNAs, suggesting that it could act as negative regulator of pathologic inflammation (19). Furthermore, developmental deletions of HuR in mice demonstrated its involvement in cellular differentiation, maturation, and migration (23–25), potentially also affecting inflammatory responses. Here we aim to clarify the role of HuR in inflammation by genetic ablation in innate immune cells and to uncover its function in macrophage control and migration that is required for the maintenance of inflammatory homeostasis and protection against cancer.

Results

Myeloid loss of HuR sensitizes mice to systemic inflammation. To examine the role of HuR in innate inflammatory responses, we induced autosomal inactivation of the *Elavl1* locus in mouse myeloid lineage. Mice expressing Cre recombinase by a lysozyme M promoter (*LysMCre*$^+$; ref. 26) were crossed to mice bearing a loxP-flanked allele (*Elavl1*$^{fl/fl}$; ref. 24 and Supplemental Figure 1A; supplemental material available online with this article; doi:10.1172/JCI45021DS1). Single- and double-heterozygote mice expressed comparable levels of HuR in macrophages; hence, we present *LysMCre*$^+$*Elavl1*$^{fl/+}$ and *LysMCre*$^-$*Elavl1*$^{fl/fl}$ as controls for *LysMCre*$^+$*Elavl1*$^{fl/fl}$ mice (referred to herein as MKO mice). Contrary to the proposed involvement of HuR in hematopoiesis (23), we did not detect numerical changes in bone marrow progenitors from MKO mice; the capacity of these progenitors to differentiate in culture confirmed that myelopoiesis occurs normally in MKO mice (Supplemental Figure 1, C–F). Recombination of the *Elavl1* locus in MKO mice was restricted to late stages of myelopoiesis, suggesting that it did not affect the ontogeny of early progenitors. Mature myeloid populations were 75%–95% devoid of HuR protein, with macrophages being the most deficient subset. MKO mice possessed a higher content of macrophages in their blood and peritoneal cavities, but other immune subsets were within physiologic range (Supplemental Figure 1B and Supplemental Figure 2).

To examine the involvement of HuR in systemic inflammatory responses, MKO mice were tested for sensitivity to endotoxemia. In this model of septic shock, systemic administration of bacterial LPS causes acute activation of innate immunity and secretion of inflammatory mediators. Outcomes range from mild fever to lethal shock, depending on LPS dose and genetic background of the host. In our setting, mice in susceptible (mixed C57BL/6J, 129Ola) or more resistant (inbred C57BL/6J) genetic backgrounds where challenged with doses of LPS and monitored for survival (Figure 1A). MKO mice on a susceptible genetic background showed a complete lethal response to an otherwise sublethal dose of LPS (600 μg). Similarly, on the resistant background, MKO mice displayed a sublethal response, in contrast to the marginal response of controls. The endotoxic response of control mice correlated with a decrease in the HuR content of macrophages (Supplemental Figure 3A). On the other hand the sensitivity of MKO mice correlated with the enhanced content of TNF, IL-6, IL-1β, and IL-12 — but not of IL-10 or TGF-β — in their sera (Figure 1B), confirming the induction of an exacerbated proinflammatory response. Thus, loss of myeloid HuR sensitizes mice to systemic pathologic inflammation.

Myeloid loss of HuR alters progression of colitis and sensitizes mice to colitis-associated cancer. To extend our observations to organ-specific inflammation, we employed a mouse model of colitis induced by dextran sodium sulfate (DSS). C57BL/6J MKO mice were used in the following studies. Oral exposure of control mice to DSS induced symptoms of acute intestinal inflammation (weight loss, diarrhea, and rectal bleeding) from day 4. Symptoms peaked around days 8–9 and, after DSS removal, returned to baseline values around day 18. A second dose of DSS on day 20 induced a milder yet prolonged response that peaked around day 28 and returned to baseline around day 40. Exposure of MKO mice to similar conditions revealed differences in colitis onset, severity, and progression (Figure 2A). Acute symptoms in mutant mice appeared on day 2, peaked on days 4–6, and rapidly returned to baseline, after DSS removal, by day 15. Histologically, the early disease activity in MKO mice correlated with faster recruitment of HuR$^-$ inflammatory cells in the mucosa, supporting epithelial damage, even on the second day of DSS administration (Figure 2,

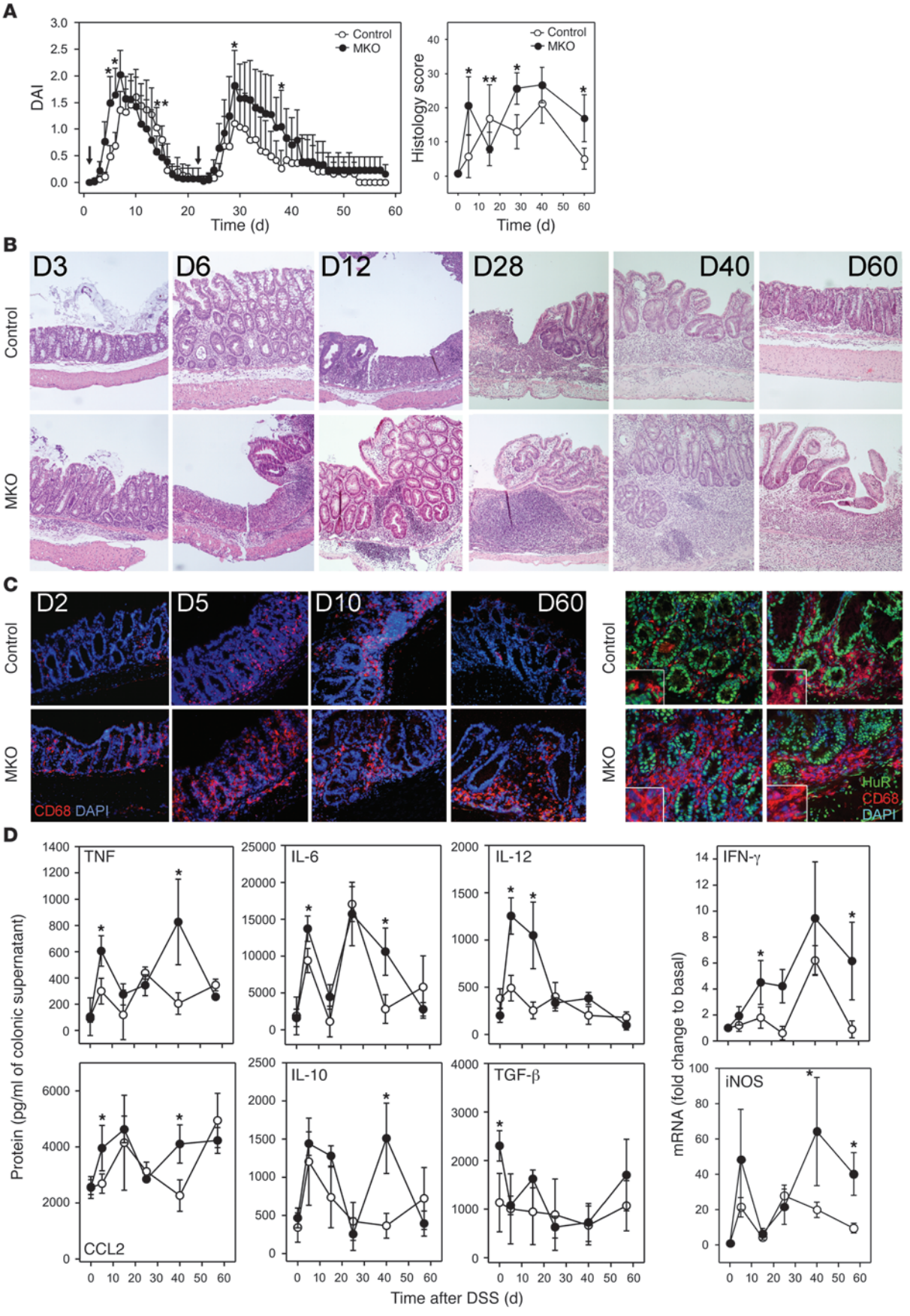
A
DAI
Control
MKO
Time (d)
Histology score
Control
MKO
Time (d)
B
D3
D6
D12
D28
D40
D60
Control
MKO
C
D2
D5
D10
D60
Control
MKO
CD68 DAPI
Control
MKO
HuR
CD68
DAPI
D
Protein (pg/ml of colonic supernatant)
TNF
IL-6
IL-12
IFN-γ
CCL2
IL-10
TGF-β
iNOS
mRNA (fold change to basal)
Time after DSS (d)

Figure 2
Myeloid deletion of HuR augments the severity and the chronicity of inflammation in a model of inflammatory bowel disease. (**A**) Macroscopic DAI (left) and histopathological evaluation of intestinal sections (right) after 2 rounds of DSS administration (arrows) in control and MKO mice. Line graphs depict mean values ± SD. n = 18–23 mice per group. *$P \leq 0.05$ for higher MKO values. **$P \leq 0.05$ for lower MKO values. (**B**) Representative histology of colonic tissue from control and MKO mice between days 3 and 60 of the DSS protocol, indicating the rapid induction of inflammation in the acute phase and its persistence after day 50. Photomicrographs of paraffin-embedded sections stained with H&E or DAB/hematoxylin. Original magnification, ×100. (**C**) Left: Detection of macrophage infiltrates in acute (Days 2–10) and chronic resolving phases (Day 60) of DSS-induced colitis via the detection of $CD68^+$ macrophage marker in sections from control and MKO mice treated with DSS. Nuclear DAPI staining indicates tissue organization. Original magnification, ×100. Right: Immunohistochemical detection of macrophage-HuR content in cryostat sections from inflamed control and MKO colons via detection of CD68 (red), HuR (green), and DAPI (blue) stainings. Original magnification, ×200 (insets ×400). (**D**) Detection of inflammatory molecules in inflamed colons from control and MKO mice either as secreted proteins from cultured organ cultures and ELISA or as mRNAs in extracts and qRT-PCR.

A–C); this was followed by rapid remission of inflammation and early presence of proliferating and regenerating crypts (Supplemental Figure 4A). In the second phase, MKO mice showed a higher disease activity index (DAI), which persisted past day 50. This aggravated response was marked by macrophage and lymphoid infiltrates, supporting the presence of ulcerations even after day 60. Colonic cultures and RNA extracts from MKO mice revealed local augmentations in proinflammatory TNF, IL-6, CCL2, and *iNos* mRNA; regulatory IL-10; and a continuum of cells expressing high IL-12 protein and *Ifnγ* mRNA suggestive of a chronic M1/Th1 bias (Figure 2D). Thus, loss of myeloid HuR induces a polarized proinflammatory response that enhances progression and maintenance of inflammatory colitis.

Notably, 2 of 19 MKO mice developed neoplastic transformations between days 48 and 60 (Supplemental Figure 4B). Thus, we tested whether myeloid HuR regulates inflammatory tumorigenesis using a mouse model of colitis-associated cancer (CAC) induced by dimethylhydrazine (DMH) and DSS. DMH is a procarcinogen that induces tumors in distal colon of rodents. The incidence of DMH-induced tumors is enhanced by chronic inflammation. Control and MKO mice receiving DMH alone remained tumor free for a period of at least 4 months (data not shown). In contrast, the incidence and number of tumors were considerably higher in MKO mice receiving both DSS and DMH compared with control groups, and tumors extended from distal to middle colon (Figure 3, A, B, and G). Tumors in MKO mice were larger in size, reflecting enhanced proliferation and higher grading, and were mostly adenocarcinomas with a high degree of dysplasia and varying degrees of inflammatory infiltration (Figure 3, C–G). Taken together, our results demonstrated that loss of myeloid HuR alters inflammation to support tumorigenesis.

HuR-deficient macrophages respond properly to activating and polarizing signals but exhibit exacerbations in inflammatory cytokines. The pathologic response of MKO mice could arise from aberrant activation of innate cell subsets. Bone marrow–derived macrophages (BMDMs) from these mice expressed αM integrin (CD11β), F4/80 macrophage antigen, Fcγ receptors (CD16/32), and key Toll-like pattern-recognition receptors; were capable of pinocytosis and phagocytosis; did not show signs of death; and signaled properly following TLR engagement, as indicated by the activation of stress signals that target ARE mRNAs, such as ERK, p38, and AMPKs, STAT3, or the MKP1 phosphatase (refs. 13, 27, 28, and Supplemental Figure 5). Thus, the loss of HuR did not affect the basic machinery for macrophage activation and function.

Next, we hypothesized that the loss of HuR altered the expression of macrophage products that favor pathologic inflammation-like cytokines involved in proinflammatory or regulatory responses. Quantitative RNA and protein analysis of cultured MKO macrophages (Figure 4, A and B, and Supplemental Figure 6) demonstrated changes in key inflammatory mediators that could support inflammatory pathologies (29) and included augmented accumulation of *Il6* mRNA and IL-6 protein secretion, a key acute-phase protein and mediator of CAC; similar response of IL-12, which drives inflammatory Th1 responses in systemic and intestinal inflammation; and augmented response of proinflammatory TNF protein — but not of *Tnf* mRNA — which is determinant in many inflammatory conditions. Surprisingly, IL-1β and COX2 proteins were reduced, which is in compliance with their negative or minimal roles in CAC (30, 31). On the other hand, anti-inflammatory TGF-β1 and IL-10 proteins were upregulated in the same cultures.

At the functional level, these changes could reflect a lack of polarization between classical inflammatory (M1) or alternative (M2) macrophage states, aberrations in signal transduction, or direct changes in the biosynthesis of effector molecules. To examine macrophage polarization, we cultured macrophages with IFN-γ for M1, or IL-4 for M2 polarization. In control macrophages these lymphokines reduced *Elavl1* mRNA, and representation of HuR^{hi} expressing subsets, under basal but not activated conditions; furthermore, IL-4 increased the cytoplasmic content of HuR (Supplemental Figure 3, B–D), suggesting that it could be involved in polarization. However, examination of specific markers and cytokine profiles revealed that HuR^- macrophages were able to be polarized, even if cytokines like TNF and IL-10 displayed altered expression (Supplemental Figure 8). As previously reported (32), IL-10 induced the *Elavl1* mRNA but decreased total and cytoplasmic HuR in control cells; however, HuR was not required for the antiinflammatory properties of IL-10 since its exogenous addition could suppress inflammatory mediators in MKO macrophages (Supplemental Figures 3 and 9). Similarly, pharmacological inhibition of MAP/SAP, PKC, or PI3Ks or agonistic AMPK activation, all of which reciprocate antiinflammatory signaling (8, 13, 27, 33) decreased cytokine expression to a similar extent (Supplemental Figure 9). From these results, we conclude that HuR acts in an autonomous fashion to regulate production of inflammatory mediators.

HuR-deficient macrophages exhibit enhanced chemotaxis to CCR2 signals. To identify additional changes induced by the loss of HuR, we used RNA from LPS-stimulated HuR^+ and HuR^- macrophages in comparative microarray hybridizations. Most expression differences were detected 2 hours after stimulation. Arguing against the role of HuR as a stabilizer, many mRNAs increased in HuR^- cells (Figure 4C) and encoded for inflammatory mediators, complement, ECM remodeling enzymes, and intracellular signaling factors (Supplemental Table 1). The list was also enriched in proinflammatory chemokine mRNAs such as *Cx3cl1*, *Cxcl9*, and *Cxcl11* (34). Importantly, the list contained CC chemokines *Ccl2* and *Ccl7* and their receptors, *Ccr2* and *Ccr3*, which mediate macrophage

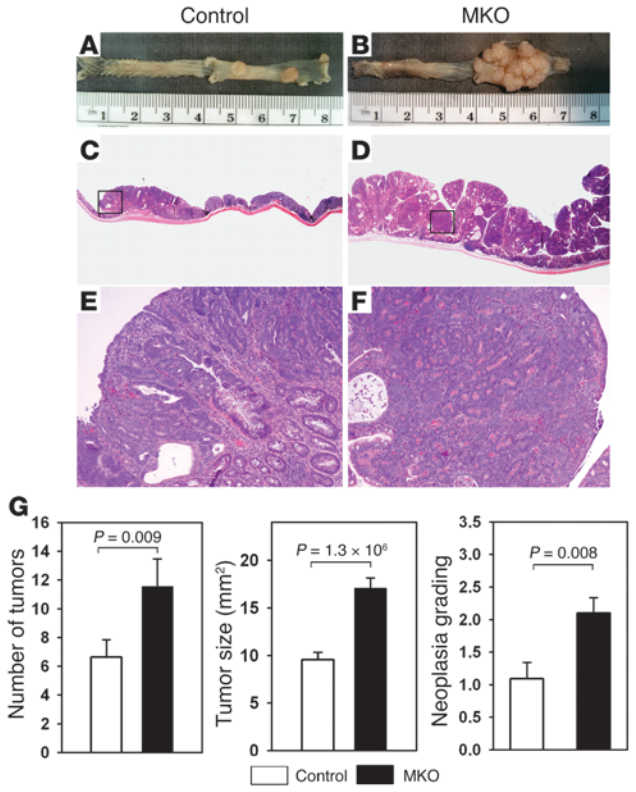

Figure 3
Deletion of HuR in myeloid cells increases susceptibility to CAC. (**A**–**F**) Comparative stereomicrographs of whole colons (**A** and **B**) and photomicrographs of colonic paraffin sections stained with H&E (original magnification, ×40 [**C** and **D**], ×200 [**E** and **F**]) from control and MKO mice sacrificed on the 15th week after induction of CAC with DSS and DMH. Note the extent of high-grade adenocarcinomas in the MKO colons. (**G**) Measurement of tumor number, size, and grading in control and MKO mice following the induction of CAC. Bar graphs depict mean values + SD from 15 mice/group.

chemotaxis in acute inflammation and cancer. CCL2 binds exclusively to CCR2, whereas CCL7 can bind to CCR1–3. Quantitative real-time PCR (qRT-PCR) confirmed the 2- to 3-fold upregulation of *Ccl2*, *Ccl7*, and *Ccr2* (but not *Ccr3*) mRNAs (Figure 4D and Supplemental Figure 6). Similarly, secretion of CCL2 and CCL7 proteins was increased in HuR$^-$ cultures (Figure 4D). Surface CCR2 was augmented in HuR$^-$ macrophages in vivo and ex vivo (Figure 4E); interestingly, the reported suppressive effect of LPS onto CCR2 expression (35) was no longer effective in these cells. To relate changes in chemokine expression to chemotaxis, mutant macrophages were tested for their migration in transwell assays (Figure 5A and Supplemental Figure 7, A and B). The migratory responses of HuR$^-$ macrophages to medium and the leukocyte-attracting chemokine CXCL12/SDF1 were similar to that of controls (Figure 5A). In contrast, HuR$^-$ macrophages displayed increased migration to recombinant CCL2, supernatants derived from activated control and MKO macrophages, and intestinal epithelial cells in the form of the CMT-93 cell line; similarly, control macrophages displayed enhanced migration to supernatants from MKO macrophages, verifying the high secretion of CCL2 by the latter. Pretreatment of control and MKO macrophages with a CCR2 antagonist (RS504393) arrested their migration to a similar extent, as did knockdown of CCL2 in intestinal epithelial cells, verifying that the migratory effect relies on these specific signals.

Autocrine and paracrine CCL2/CCR2 engagement act exclusively on macrophages to guide their migration during inflammation; thus we looked for changes in the responses of MKO mice that could phenocopy states of CCL2/CCR2 overexpression. As stated earlier, the peripheral blood of resting MKO mice possessed higher numbers of monocytes and/or macrophages. Under LPS challenge, and despite their normal representation in bone marrow, these macrophages accumulated in the blood of MKO mice in numbers that surpassed those of polymorphonuclear cells (PMNs) by 24 hours; similar to cells that overexpress CCL2, these cells were αM integrin/CD11β^{hi}, suggestive of their robust chemotactic and/or migratory response (Figure 5B and Supplemental Figure 7D). The effect of the loss of HuR in innate migration patterns was also evident in the CCR2-dependent model of thioglycollate-induced aseptic peritonitis, as assessed by the temporal representation of PMNs and monocytes in bone marrow, peripheral blood, and peritoneal cavities by means of CD11β, F4/80, and Ly6G expression (Figure 5B). In control mice, thioglycollate caused a rapid reduction of bone marrow myeloid cells by 24 hours; at the same time, PMNs were reduced in blood but increased in the peritoneum. From 48 to 72 hours, the wave of peritoneal PMN recruitment returned to basal values, followed by an increase in macrophages by 72 hours. Bone marrow values from MKO mice were invariable from those of controls (Supplemental Figure 7C), but peripheral PMN-to-macrophage ratios were completely inverted, with monocytes/macrophages migrating rapidly from peripheral blood to the cavity by 24 hours and PMNs showing a lesser response. Collectively, our data demonstrated that the inflammatory and tumor-promoting effects of the loss of HuR correlated with a rapid migration of effector macrophages and increased CCR2 signaling.

HuR as a regulator of mRNA turnover and translation. Next we used mutant macrophages to investigate the molecular effects of the loss of HuR in cytokine biosynthesis. Dysfunction of ARE-BPs such as TTP, TIA-1, KSRP, and AUF1 can result in cytokine overproduction, and HuR can cross-regulate their biosyntheses (11). However, we did not detect severe changes in the expression of such ARE-BPs in HuR$^-$ macrophages and found only a small increase in *Ttp* mRNA, possibly reflecting a counter-response (Supplemental Figure 10). Thus, the altered expression of cytokines was due to the loss of HuR and not of other known ARE-BPs.

Given that HuR was dispensable for IFN-γ, IL-4, and IL-10 signaling, we focused on the signal activating cytokine expression, i.e., LPS via TLR4. We previously used RNP IP (R-IP) assays to demonstrate that *Tnf*, *Tgfβ1*, and *Cox2*, but not *Il1β* or *Il6* mRNAs, interact with HuR in activated macrophages (19). Using the same platform, we looked for signal-induced and temporal changes in the interactions of cytoplasmic HuR with *Ccl2*, *Ccl7*, *Ccr2*, *Il10*, and *Il12* mRNAs. *Tnf* and *Il6* mRNAs were monitored as positive and negative controls, respectively. Isotype mIgG1 IP assays from HuR$^+$ BMDM extracts were used to control for binding specificity, and the quality of IP reactions was monitored by immunoblotting (Supplemental Figure 12C). We found that *Ccl2*, *Ccr2*, *Il10*, and *Tnf* mRNAs interacted with HuR under basal and inducible conditions, whereas *Il12*, *Ccl7*, and *Il6* mRNAs did not (Figure 6A). Interestingly, we noted that associations of HuR increased multifold at late times following LPS, correlating with the potential for

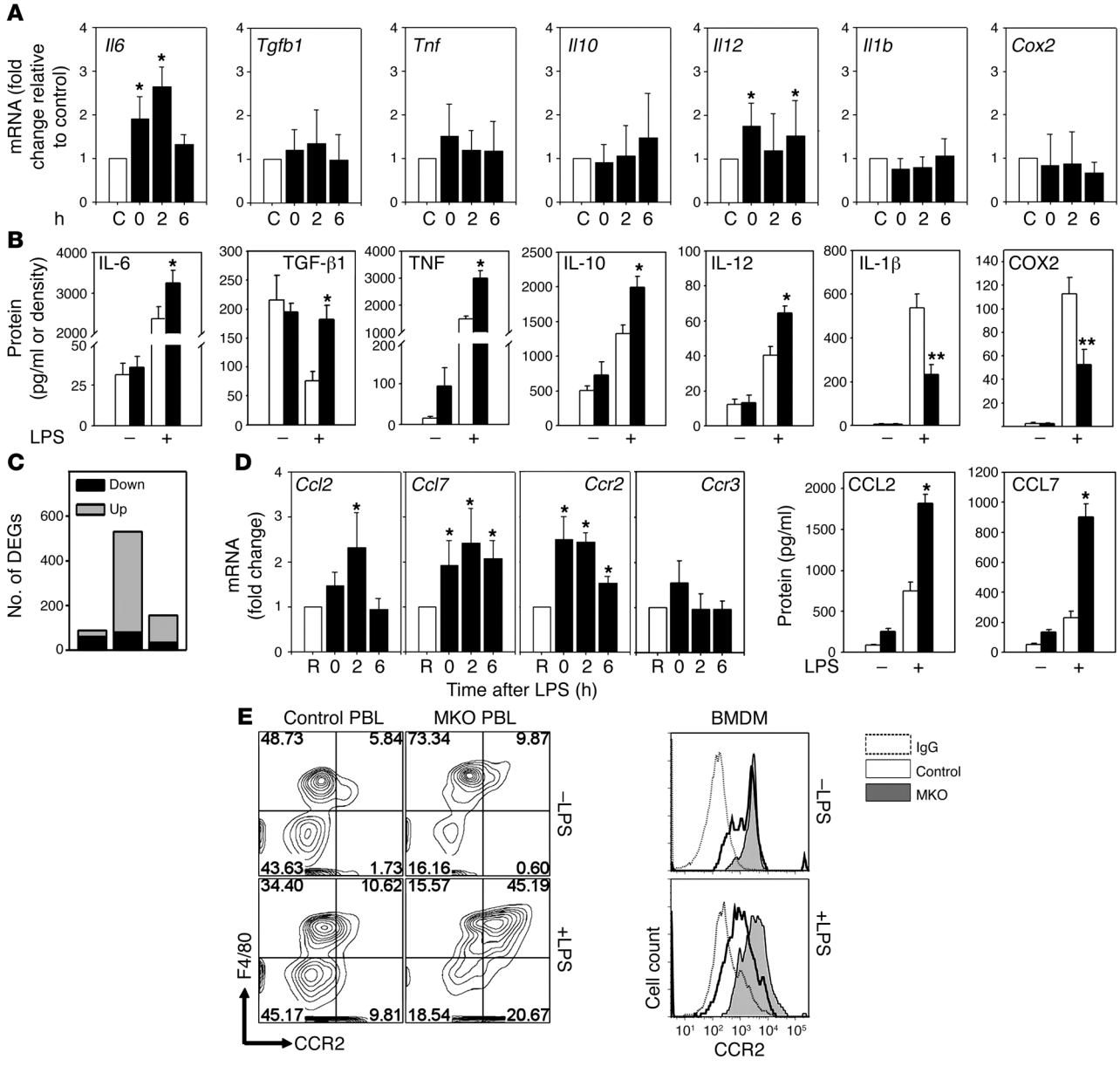

Figure 4

HuR-null macrophages show exacerbations in the biosynthesis of inflammatory cytokines and chemokines. (**A**) Bar graphs depict differences in inflammatory and immunomodulating mRNAs in HuR$^+$ and HuR$^-$ macrophages. Data are fold change +SD relative to control values (white bars) at each time point from qRT-PCR experiments using RNA from 3–5 individual cultures per genotype. (**B**) Detection of protein products corresponding to the mRNAs in **A**, in control (white bars) or MKO (black bars) macrophages. Soluble factors were detected in culture supernatants before and after stimulation of macrophages with LPS. Data (pg/ml or density units + SD) were derived from 3 experiments, each with 4–5 individual cultures per genotype. (**C**) Stacking bar graph of differentially expressed genes (DEGs) in LPS-stimulated MKO BMDMs. Data were obtained from microarray hybridizations with 3 cultures/group/time point. (**D**) Bar graphs of levels of chemokine and chemokine receptor mRNAs and proteins in LPS-stimulated HuR$^-$ macrophages either as fold change compared with control mRNA values or as secreted protein values in control (white bars) and MKO (black bars) macrophage supernatants. Data are from 3 experiments, each with 4–5 individual cultures per group. (**E**) Flow cytometric detection of surface CCR2 expression on F4/80$^+$ macrophages in the peripheral blood of control and MKO mice or the corresponding cultured BMDMs and in the presence or absence of LPS for 2 and 12 hours, respectively. *$P \leq 0.05$ for higher MKO values. **$P \leq 0.05$ for lower MKO values.

HuR in cytokine suppression. As previously noted (19), HuR protein remained constant proximal to LPS stimulation. We noted, however, that LPS induced accumulation of *Elavl1* mRNA and cytoplasmic localization of HuR at 6 hours, correlating with the interaction data (Supplemental Figure 3, B–F).

Based on the above, we sought to identify effects of the loss of HuR on target mRNAs. First, we used density separation to analyze the association of mRNAs with polysomes as a measure of translation. The polysomal content in *Il10* and *Tnf* mRNAs increased immediately after activation of control macrophages

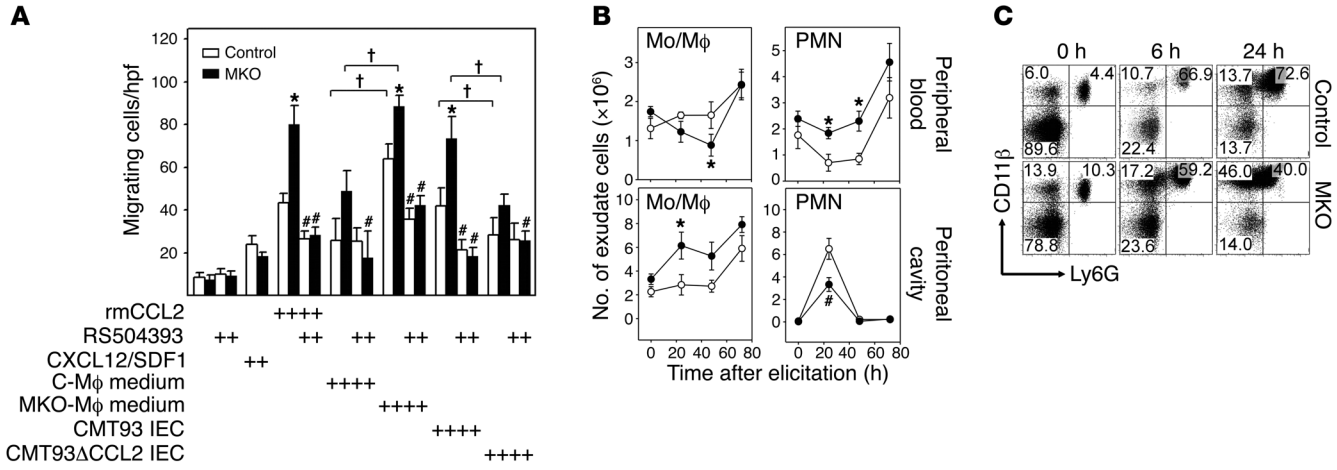

Figure 5

HuR-null macrophages exhibit increased chemotactic responses and migration profiles. (**A**) Chemotaxis of control and MKO macrophages, as untreated or treated (plus signs) with RS504393, recombinant CCL2, CXCL12, control (C-MΦ) and MKO (MKO-MΦ) macrophage supernatants or CMT93 epithelial cells (IECs) containing or lacking CCL2 (see also Supplemental Figure 6). Values reflect migrating cells per HPF of transwell membranes. Data are from at least 2 independent experiments, each with 3 replicas per genotype. (**B**) Numbers of monocytes/macrophages (Mo/MΦ) and PMNs in the peritoneal cavity of control (white circles) and MKO (black circles) mice during aseptic peritonitis. Values were derived from flow cytometric detection of CD11b and Ly6G/Gr1. Graphs depict mean values (±SD) from 3 experiments, each with 3 mice per time point. (**C**) Detection and quantitation of Mo/MΦ ($CD11b^+Ly6G^-$) versus PMNs ($CD11b^+Ly6G^+$) in peripheral blood of control and MKO mice following LPS challenge. Representative dot plots from 2 independent experiments are shown. $^*P < 0.05$ versus control; $^\#P < 0.05$, RS504393-treated versus untreated control or MKO; $^\dagger P < 0.05$, control versus MKO medium, or cells containing versus lacking CCL2.

and was enhanced in MKO cells (Figure 6B and Supplemental Figure 12A); a similar effect was observed for *Ccr2* mRNA at 6 hours, whereas the opposite was observed for *Cox2* mRNA. LPS induced a transient decrease in the translation of *Ccr2* and *Tgfb* mRNAs in control macrophages; however this effect was not observed in MKO cells. Thus HuR acts to modify the translation of specific inflammatory mRNAs.

Next, we looked for changes in mRNA half-lives following transcriptional inhibition by actinomycin D as a measure of mRNA stability or decay. This approach revealed that *Ccl2* and *Ccr2* mRNAs, but not *Tnf* and *Il6* mRNAs, were more stable in stimulated MKO macrophages, providing an explanation for their augmented accumulation (Figure 6C and Supplemental Figure 12B). To verify this, we examined mRNA turnover in macrophages from mice overexpressing a doxycycline-inducible (Dox-inducible), HA-tagged form of human HuR in macrophages (*TgLrTtA-HAHuRL.632*, referred to as $Tg632^+$ for simplicity). As reported in ref. 19, *Tnf* mRNA increases in activated $Tg632^+$ macrophages, but its protein output decreases. Conversely, *Ccr2* mRNA decreases in the same cells, mirroring the effect in MKO cells. Interestingly, and despite a substantial block in CCL2 protein, the accumulation of its mRNA was minimally affected by HuR overexpression, demonstrating prevalence in translational inhibition (Supplemental Figure 11). In terms of turnover, overexpression of HuR increased the stability of *Tnf* but not of *Ccl2* or basal *Ccr2* mRNAs; however, it reduced the stability of *Ccr2* mRNA following LPS stimulation (Figure 6C).

Because the lack of a clear effect on *Ccl2* mRNA turnover in $Tg632^+$ cells might be due to saturation effects in the association of *Ccl2* with HuR, we employed an alternative approach. Given that major determinants of posttranscriptional control reside within 3′UTRs, we tested whether HuR affected UTR-mediated degradation in a cell-free system. Uniformly ^{32}P-labeled, capped and polyadenylated RNAs containing mouse *Ccl2*, *Ccr2*, and *Tnf* 3′UTRs or a fragment of *Gapdh* mRNA were added to cytosolic (S100) extracts from activated macrophages. Reactions were performed until *Gapdh* values started to decline (Figure 6, D and E). The decay of *Tnf* 3′UTR RNA was similar in control and MKO extracts but increased in activated $Tg632^+$ extracts. In sharp contrast, the decay of *Ccl2* and *Ccr2* 3′UTR RNA increased in MKO extracts and decreased in activated $Tg632^+$ extracts. We conclude that HuR regulates the homeostasis of inflammatory responses by suppressing cytokine and chemokine mRNA turnover and translation.

HuR binding to UTR domains affect mRNA use under inflammatory stimulation. Next we looked for discrete regions interacting with HuR on *Ccl2* and *Ccr2* 3′UTRs to mediate suppression using EMSAs with specific probes and recombinant GST-HuR (Figure 7B). *Tnf* 3′ARE was used as positive control. A single strong complex was formed with the first 66 nucleotides of *Ccl2* 3′UTR. Interactions with *Ccr2* 3′UTR were detected in 3 discrete locations: high-affinity complexes were detected in the first 300 nucleotides (nucleotides 1252–1551) and low-affinity interactions were detected in the adjoining fragment (nucleotides 1551–1852) and the last 247 nucleotides (nucleotides 2752–2999) (Figure 7A). Informatic analysis revealed that these domains possessed putative HuR consensus sites (Supplemental Table 2).

To confirm a suppressive effect of HuR/UTR interactions, we engineered a series of UTR sensors, in which full-length *Ccl2*, *Ccr2*, *Tnf*, and *Gapdh* UTRs and 5′ truncated forms of *Ccl2* and *Ccr2* UTRs lacking strong affinity domains (Δ forms) were fused to *GFP* mRNA, thus allowing for carrier cells and protein levels to be measured by GFP fluorescence. These were delivered into BMDM by means of a lentiviral vector that uses a CMV promoter to drive transcription. Differentiated BMDMs could not be transduced, and so bone marrow progenitors were infected during their differentiation to BMDMs. The *Gapdh* sensor yielded comparable transduction efficiencies and GFP intensities across treatments and genotypes

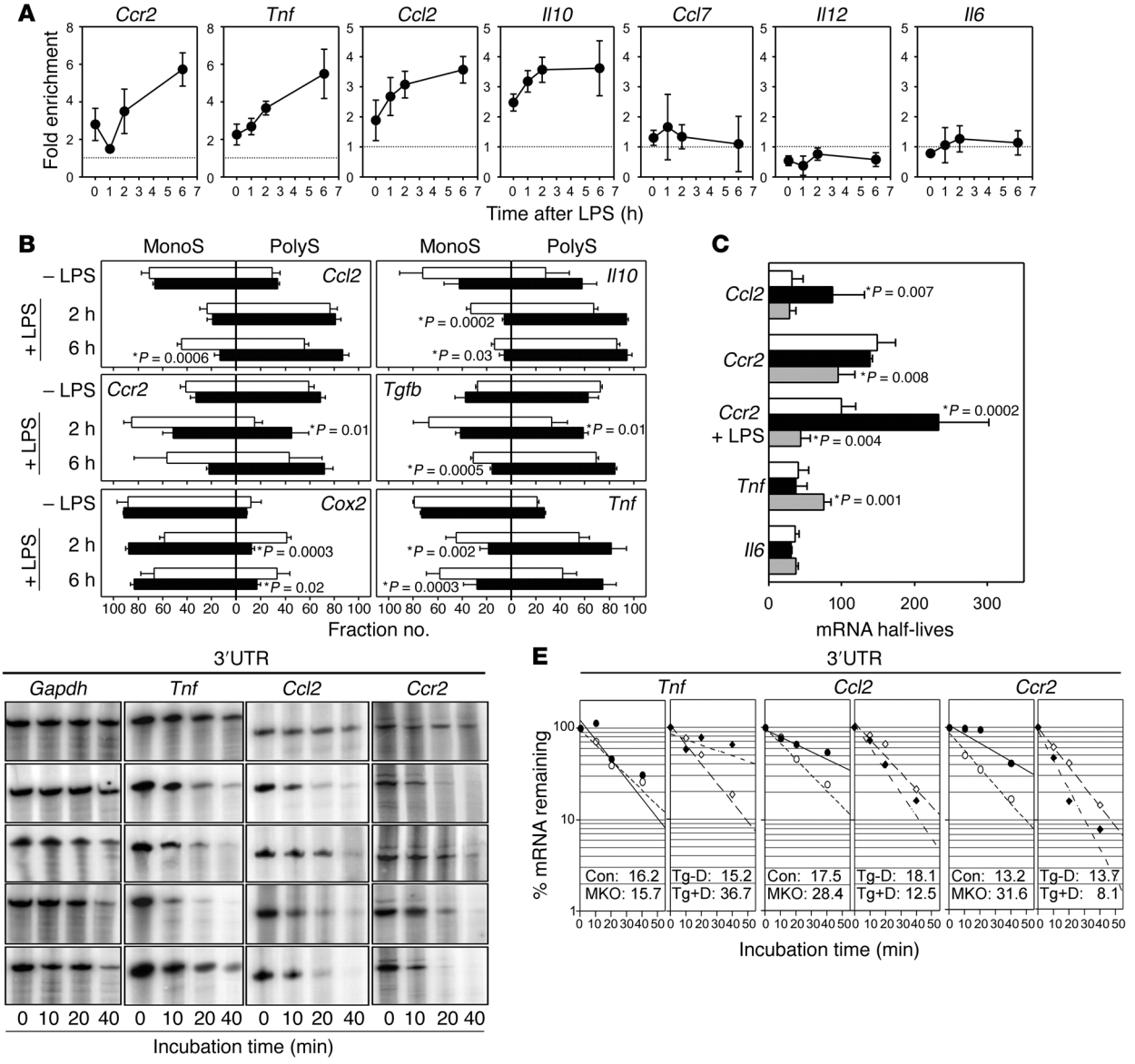

Figure 6

HuR targets selective posttranscriptional processes to maintain the balance in inflammatory reactivity. (**A**) qRT-PCR detection of selected mRNAs tested to IP with HuR at different time points following LPS stimulation of HuR$^+$ macrophages. Data (biological triplicates ± SEM) are represented as fold enrichment of each mRNA in HuR-IP samples compared with its abundance in IgG1-IPs. Enrichment levels were adjusted to *Gapdh* mRNA. Enrichments above cut-off value (dotted line) were considered significant. (**B**) qRT-PCR detection of HuR-interacting mRNAs in monosomal/polysomal fractions from macrophages as resting or LPS-treated (2 and 6 hours). Data from measurements (±SD) in individual fractions normalized to *Gapdh* mRNA and presented as total monosomal or polysomal percentages of cytoplasmic RNA. *$P < 0.05$, control (white bars) versus MKO (black bars). (**C**) Changes in the LPS-induced turnover of *Ccl2*, *Ccr2*, *Tnf*, and *Il6* mRNAs or basal *Ccr2* mRNA in actinomycin D–treated control (white bars), HuR$^-$ (black bars), and HuR-overexpressing (gray bars) macrophages. Data are half-lives (±SD) derived from decay plots from 3 independent experiments. *$P < 0.05$ versus control (see also Supplemental Figure 12). (**D**) In vitro regulation of the stability of ^{32}P-labeled mRNAs containing *Ccl2*, *Ccr2*, and *Tnf* 3′UTR incubated with S100 extracts from activated control, MKO, and Dox-treated *Tg632*$^+$ macrophages. RNAs were incubated for various times, resolved on denaturing gels, and visualized via autoradiography. (**E**) Semilogarithmic quantitation was performed using normalization to nontreated probe (mock) and the *Gapdh* mRNA. Circles indicate values from control or Tg–D (white) or from MKO or Tg+D (black) extracts. Representative half lives from at 2–4 experiments are indicated.

(Figure 7, C and D). A small percentage of GFP^{lo} BMDMs could be generated with the *Tnf* 3′UTR sensor, but percentages and fluorescence intensities increased in control and MKO BMDMs following LPS by 2-fold and 4-fold, respectively, but not in *Tg632*$^+$ BMDMs. Similar observations were made for the *Ccl2* 3′UTR sensor, with the exception that its basal levels were lower in MKO BMDMs. In contrast, the truncated *Ccl2* 3′UTRΔ sensor yielded an invariable distribution of signals across genotypes and treatment regimes. Transduction of the *Ccr2* 3′UTR sensor yielded high and comparable values in control and MKO macrophages but a near 50%

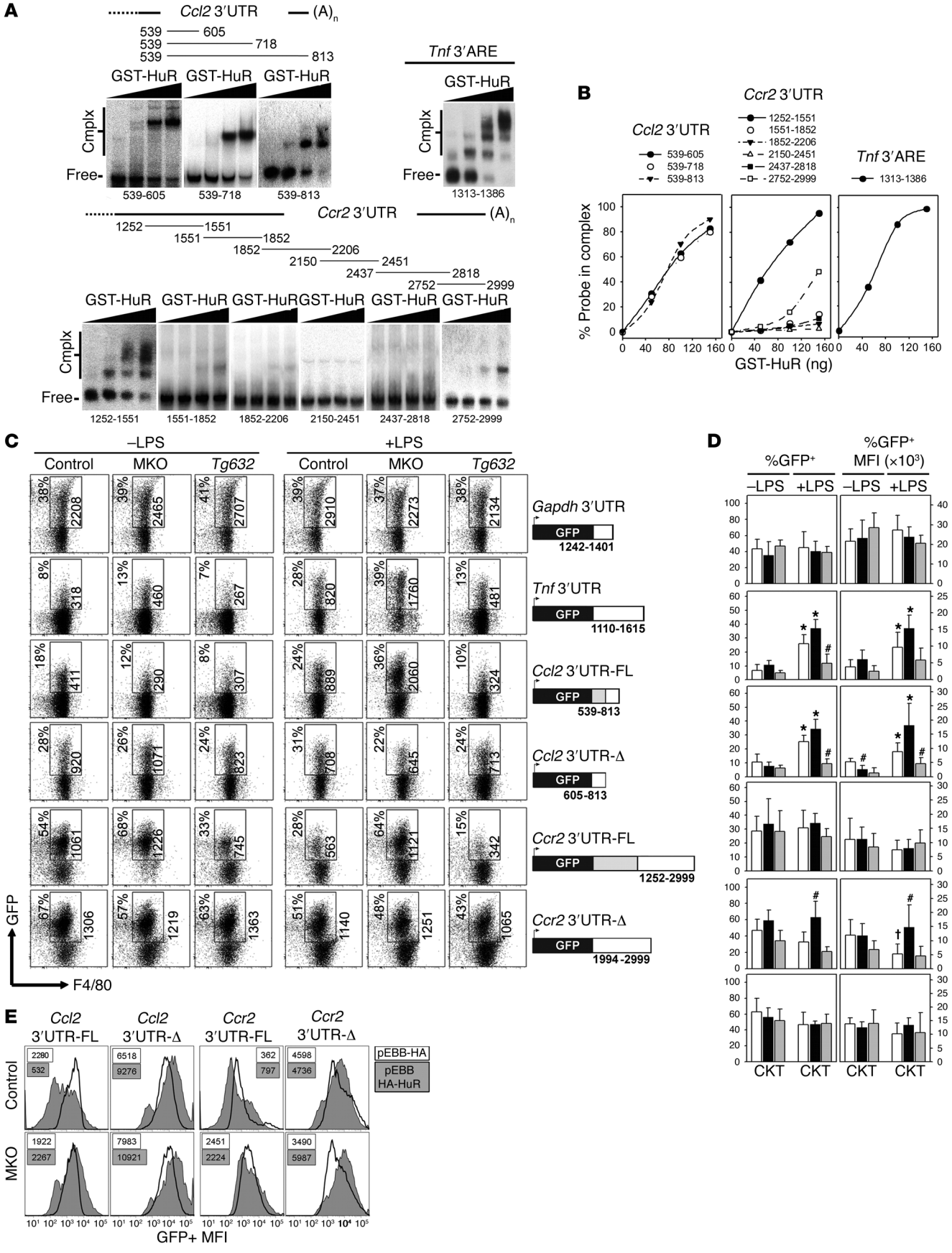
A
Ccl2 3′UTR
(A)n
539 605
539 718
539 813
GST-HuR GST-HuR GST-HuR
Cmplx
Free-
539-605 539-718 539-813
Tnf 3′ARE
GST-HuR
1313-1386
Ccr2 3′UTR
1252 1551
1551 1852
1852 2206
2150 2451
2437 2818
2752 2999
GST-HuR GST-HuR GST-HuR GST-HuR GST-HuR GST-HuR
1252-1551 1551-1852 1852-2206 2150-2451 2437-2818 2752-2999
B
Ccl2 3′UTR
539-605
539-718
539-813
Ccr2 3′UTR
1252-1551
1551-1852
1852-2206
2150-2451
2437-2818
2752-2999
Tnf 3′ARE
1313-1386
% Probe in complex
GST-HuR (ng)
C
–LPS
+LPS
Control MKO Tg632 Control MKO Tg632
Gapdh 3′UTR
GFP
1242-1401
Tnf 3′UTR
1110-1615
Ccl2 3′UTR-FL
539-813
Ccl2 3′UTR-Δ
605-813
Ccr2 3′UTR-FL
1252-2999
Ccr2 3′UTR-Δ
1994-2999
GFP
F4/80
D
%GFP+
%GFP+ MFI (×10³)
–LPS +LPS –LPS +LPS
CKT CKT CKT CKT
E
Ccl2 3′UTR-FL
Ccl2 3′UTR-Δ
Ccr2 3′UTR-FL
Ccr2 3′UTR-Δ
Control
MKO
pEBB-HA
pEBB HA-HuR
GFP+ MFI

Figure 7
HuR targets specific UTR domains to limit the inducible use of cytokine/chemokine mRNAs. (**A**) Identification of 3′UTR domains from *Ccl2* and *Ccr2* mRNAs binding to HuR. RNA-EMSA with ^{32}P-labeled RNA probes containing fragments of *Ccl2*, *Ccr2*, and *Tnf* 3′UTRs in the presence of increasing quantities of recombinant GST-HuR. Protected fragments and free probes are indicated. (**B**) Representative quantitation of HuR binding to the RNA probes presented in **A**. Percentages of radiolabeled probe in complex with HuR was determined and expressed as a percentage of the total (shifted added to free). (**C**) Bone marrow cells from control, MKO, and *Tg632*$^+$ mice were transduced with UTR sensor constructs. Untreated or LPS-treated BMDMs were analyzed by flow cytometry. Shown are percentages of GFP$^+$ cells in F4/80$^+$ macrophages (left) and mean fluorescence intensities of these cells (right). (**D**) Enumeration of GFP$^+$ macrophages as percentages and fluorescence values from control (white bars), MKO (black bars), and *Tg632*$^+$ (gray bars) macrophages compiled from 2–3 experiments. $^*P < 0.05$ versus untreated; $^\#P < 0.05$ versus control; $^\dagger P < 0.05$ versus untreated controls. (**E**) Effect of transient HA-HuR expression in MEFs containing UTR sensors. Shown are cytometric histograms depicting GFP levels as mean fluorescence intensity values from control and MKO MEFs bearing pEBB-HAHuR or control plasmids.

reduction in *Tg632*$^+$ BMDMs. LPS reduced GFP signals in control and *Tg632*$^+$ BMDMs but did not affect MKO values. Finally, the truncated *Ccr2* 3′UTRΔ sensor yielded the highest representation and intensity of signals across genotypes and remained unaffected by LPS. To validate the effects of HuR in a system devoid of changes in transduction efficiencies, we used FACS sorting to isolate clonal HuR$^+$ and HuR$^-$ mouse embryonic fibroblasts (MEFs) bearing UTR sensors. MEFs stably expressing *Tnf* 3′UTR sensors could not be established, suggesting a nonpermissive effect of this UTR. We noted that the intensity of the *Ccl2* 3′UTR sensor appeared lower in HuR$^-$ than in HuR$^+$ MEFs as in resting BMDMs; in contrast, *Ccr2* 3′UTR was expressed as highly in HuR$^-$ MEFS as it was in BMDMs. We also noted that truncated sensors exceeded the intensities of their full-length counterparts irrespective of genotype. Given that these differences could arise also from integration, clonal effects, or tissue-restricted effects, we focused on qualitative differences induced by transfecting an HA-tagged HuR expression vector (Supplemental Figure 13). Exogenous addition of HuR decreased the expression of full-length UTR sensors in HuR$^+$ MEFs but not in HuR$^-$ MEFs nor in MEFs possessing truncated UTR sensors (Figure 7E). Collectively, our data demonstrate that HuR recognizes discrete domains in inflammatory mRNAs to promote their signal-induced silencing against pathologic inflammation.

Myeloid overexpression of HuR protects mice from colitis and CAC. Our current data suggest that HuR overexpression can attenuate intestinal inflammation and cancer. To test this, *Tg632*$^+$ transgenic mice were assayed for susceptibility to colitis and CAC. In pilot experiments we determined an oral dose of Dox that could induce transgenic HuR in vivo without affecting colitis in non-transgenic groups (data not shown). Additional controls included untreated *Tg632*$^+$ mice. Strikingly, and in contrast to all control groups, the 2 rounds of DSS induced only a small and transient inflammatory response in the colons of Dox-induced *Tg632*$^+$ mice, with several mice showing macroscopically undetectable responses (Figure 8, A and B). Most importantly, DSS/DMH treatment of induced *Tg632*$^+$ mice yielded the appearance of a few adenomas that were small in size and low grade compared with the adenocarcinomas in control groups (Figure 8, C and D). Our data emphasize the therapeutic potential of HuR and demonstrate that strategies aimed at increasing HuR functions in innate effector cells can be effective against pathologic inflammation and cancer.

Discussion

In this study we assessed the role of HuR in inflammation using a knockout in the murine myeloid lineage. HuR was dispensable for late development of innate immune cells and induction of inflammatory signals; however, it was essential for the balance of proinflammatory and homeostatic states governing the extent of the inflammatory response.

Previously, we reported that the overexpression of HuR could block selected macrophage-derived cytokines and attenuate an acute inflammatory reaction (19), suggesting that it could act as a negative regulator of inflammatory mRNAs. This was confirmed by the myeloid deletion of HuR, which induced exacerbations in proinflammatory cytokines and sensitivity to acute inflammatory reactions such as endotoxemia. Furthermore, the aggravation of modeled colitis in mutant mice revealed that HuR specifically controls proinflammatory innate responses. We attributed the inflammatory effects of the loss of HuR to qualitative and quantitative changes in molecules that were typical of the continuum from proinflammatory to resolving states. Upon inflammatory stimulation, HuR$^-$ macrophages acquired a TNF^{hi}IL-6^{hi}IL-12^{hi}NO$^+$ phenotype suggestive of an exacerbated M1 response (1, 2). Interestingly, these cells were also IL-10^{hi}TGF-β^{hi}IL-1β^{lo}COX2^{lo}, reminiscent of an M2 profile (1, 2, 36). However, HuR$^-$ macrophages could be polarized in vitro, suggesting that cytokine discrepancies resulted from biosynthetic defects and/or compensating relationships in cytokine networks.

The consequences of the amplified proinflammatory character of HuR$^-$ macrophages were revealed by the sensitivity of mutant mice to CAC. Many reports implicated HuR in colon cancer (17, 37–39) but did not focus on the inflammatory component of the process. Epidemiological, clinical, and transgenic studies established a link between inflammation and cancer and highlighted inflammatory and tumor-associated macrophages (TAMs) as central players in tumor initiation and progression (4, 5). In the context of chronic inflammation, macrophages release cytotoxic molecules, which cause epithelial DNA damage and epigenetic aberrations toward premalignant transformation (4, 5). Furthermore, the increased production of TNF and IL-6 provides growth and expansion signals to tumor progenitors and augments tumor formation (4). Once tumors develop, TAMs respond to a hypoxic tumor environment and promote tumor growth by secreting factors that aid tissue remodeling (e.g., MMP9), angiogenesis (VEGFs), and immune modulation (IL-10 and TGF-β). Many of these factors appear upregulated in HuR$^-$ macrophages and correlate with increased tumor size and grade in CAC-treated mutant mice.

The functions of inflammatory macrophages vary according to their migration, invasion, and retention patterns, which are in turn tightly regulated by chemokine and chemokine receptor interactions (34). As shown herein, HuR$^-$ macrophages displayed alterations in specific chemokines guiding inflammatory recruitment, such as CCR2 and 2 of its ligands, CCL2 and CCL7. Although not addressed in vivo, the increased migration of HuR$^-$ macrophages toward autocrine and paracrine sources of CCL2, the attenuating effect of CCR2 inhibition, and the rapid recruitment of HuR$^-$ macrophages to sites of inflammation are suggestive of a HuR/CCL2/CCR2 axis in inflammation and cancer control. Clinical studies and mouse mutants have defined CCL2 as an exclusive and potent

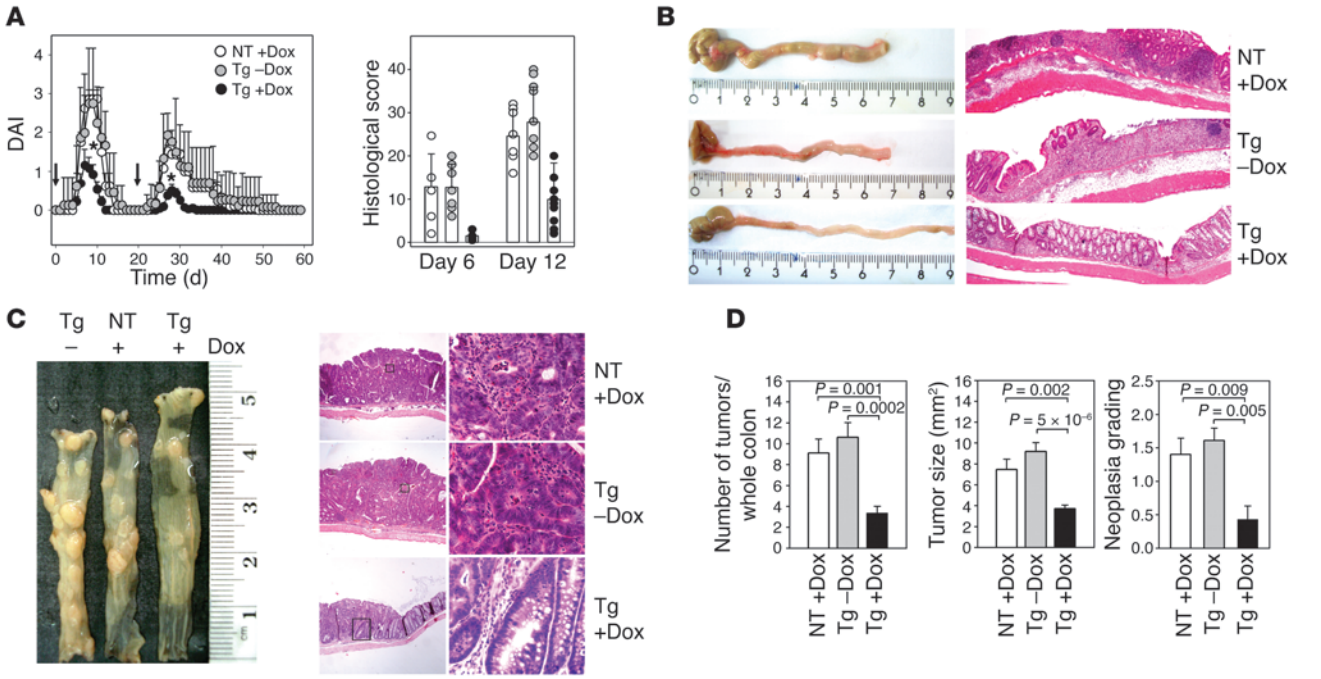

Figure 8

Inducible overexpression of HuR in myeloid cells delays the onset and severity of inflammatory bowel disease and attenuates CAC. (**A**) DAI and histopathological scoring of intestinal sections following induction of DSS-induced colitis in control (nontransgenic [NT] or *Tg632*$^+$ [Tg] mice) and Dox-activated transgenic mice. Line and bar graphs depict mean values +SD from 14–16 mice per group. *$P \leq 0.05$. (**B**) Photographs of large intestines and histology from control and activated *Tg632*$^+$ mice on day 10 of the DSS protocol. Note the near absence of swelling/shortening of the large intestine, and the lack of extensive submucosal inflammation in activated transgenic mice. Original magnification of H&E-stained photomicrographs, ×40. (**C**) Comparative stereomicrographs and colonic sections (H&E stained; original magnification, ×40 [left], ×400 [right]) indicating the nearly complete absence of neoplasias in activated *Tg632*$^+$ mice following the induction of CAC. (**D**) Tumor number, size, and grading in control and activated *Tg632*$^+$ colons following the induction of CAC. Bar graphs depict mean values + SD from 15 mice per group.

chemoattractant of inflammatory monocytes in human inflammatory bowel disease and cancer. Similarly, CCR2 can differentiate between inflammatory and resident monocytes and macrophages (40, 41). The overexpression of CCL2 observed in MKO mutants phenocopied the transgenic overexpression of CCL2, which enhances recruitment of inflammatory macrophages to mucosal sites and responses to bacterial infection (42–44). Conversely, HuR overexpression is phenotypically similar to CCL2/CCR2 inhibition toward the attenuation of CAC (45–47). We demonstrated that HuR is required to control *Ccl2* and *Ccr2* mRNAs by TLRs. This is of particular interest since these mRNAs respond differentially to this type of signal. Following recruitment, CCL2 is maintained at high levels, but CCR2 is downregulated, partly via decay of its mRNA (35, 48, 49), thereby blocking further influx and allowing for CCR1–CCR5–dependant positioning in the tissue (34). Herein we showed that the loss of HuR augments CCL2 production. On the other hand, the effects on CCR2 expression are more severe; the loss of HuR not only augments CCR2 expression, but it also renders it unresponsive to LPS. In that sense, it is logical to conceptualize that a fundamental difference in the chemotaxis of HuR$^-$ cells is their higher sensitivity as responders due to the elevated expression of CCR2. This supposition is further supported by the accumulation of macrophages in the periphery of unchallenged mice and their early influx in sites of inflammation that could result from their greater mobilization from bone marrow or peripheral blood, respectively.

Additional factors could support the phenotypes of MKO mice. The complex profile of HuR$^-$ macrophages did not allow assessment of direct vs hierarchical relationships between altered macrophage profiles and interplays between cytokines and migration effects. Still, our search for HuR target mRNAs suggested that these processes are under the direct control of this RBP.

The number of augmented mRNAs and proteins in HuR$^-$ macrophages and the responses of HuR-target mRNAs in macrophages argue against the actions of HuR as an exclusive post-transcriptional enhancer. Classical ARE-containing transcripts like *Tnf* and *Cox2* mRNAs appear unaffected by the loss of HuR despite their increased stability when HuR is overexpressed (19). A similar lack of response was observed for ARE-containing *Il10* mRNA and for *Tgfb* mRNA, which does not contain ARE. In contrast, *Ccl2* and *Ccr2* mRNAs accumulated more in mutant macrophages. Arguably, nuclear events affecting mRNA maturation and mediated by HuR (50) could contribute to increased mRNA accumulation. However, HuR appears to promote and not to inhibit mRNA maturation. As described herein, the effects of HuR on mRNA accumulation may include the promotion of mRNA decay under specific circumstances; this is supported by our measurements on chemokine mRNA decay and of 3′UTR-bearing reporter mRNAs in cell-free systems and transduced macrophages. We identified specific domains for the binding of HuR to *Ccl2* and *Ccr2* 3′UTRs and demonstrated the inhibitory capabilities of these 3′UTRs. For *Ccl2*, a recent report demon-

strated HUR's interaction to the human *Ccl2* 3′UTR in epithelial cells but proposed that it acts to enhance mRNA stability (33). In our studies, the interaction of HuR with a homologous domain in mouse *Ccl2* 3′UTR promoted destabilization; this discrepancy could be due to differences in signal and cell type. Even in our experiments, we noted that *Ccl2* 3′UTR reporters showed difficulties in their expression in non-activated macrophages and MEFs and that the suppressive effect of HuR toward the *Ccl2* mRNA was restricted to activated macrophages. Additional issues confine our hypothesis on the LPS-induced responses of HuR-interacting mRNAs. For example, data stemming from lentiviral transfer of reporter genes might reflect differences in relative infection efficiencies, frequency, and location of integration sites, and more. Given the difficulties in the normalization of these parameters in primary and basal cellular settings, we cannot consider the reported values to be quantitatively comparable. At a qualitative level, however, these data confirm the effects of the absence or overexpression of HuR on the inducible regulation of its target mRNAs, as revealed by decay and translation measurements.

In agreement with our previous observations (19), our current studies verify that HuR can suppress the translation of *Tnf*, *Ccl2*, *Ccr2*, and *Tgfb* mRNAs. However, several discrepancies were noted. Although the translation of *Il10* mRNA may be similarly suppressed by HuR, its biosynthesis was not reduced in HuR-overexpressing macrophages. Furthermore, the response of *Cox2* mRNA shared similarities in HuR-overexpressing to HuR-null macrophages. This surprising diversity in mRNA responses can only be explained if HuR cooperates with other cofactors to form distinct RNP complexes guided by sequence-specific elements on each mRNA. Such differential interactions could also explain the differential responses of mRNAs responding to the same signal, as in the case of the *Ccl2* and *Ccr2* mRNAs. Our initial observation of genetic synergy between HuR and TIA1 in translational suppression of *Tnf* mRNA in macrophages (19) has been followed by several reports of similar "suppressive liaisons" of HuR with RBPs and microRNAs (18, 20–22). Given recent hypotheses of co-regulation of mRNAs involved in complex cellular responses such as inflammation (7, 51), we postulate that HuR acts as a coordinator of distinct RNP associations formulated around specific cis-element codes. Such RNP associations would be altered by both the absence, presence, or overexpression of HuR as well as the signaling requirements of other RNP components, thus skewing expression outcomes and, as a consequence, cellular response. The limitations of our current experimental design precluded the identification of direct interactions between HuR and RNP or microRNA components that could affect mRNA stability and translation. Future analyses of signal induced RNP associations in a HuR-deficient setting will address the validity of our hypothesis.

The regulatory effects of HuR appear to be guided by activating signals. This is supported by the LPS-induced associations of HuR to its target mRNAs, which increased toward time points of proinflammatory cessation. Despite effects of polarizing signals on HuR protein, these signals do not require the presence of HuR. Similarly, signaling cascades, previously thought to converge at ARE-BPs and AREs, (e.g., via p38; ref. 8) functioned properly in the absence of HuR. This may suggest that in macrophages HuR is controlled in a fashion different from other RBPs (e.g., TTP; refs. 8, 10), and hence its connection to TLR signaling remains to be determined. Alternatively, the induction of *Elavl1* mRNA and its discordance to HuR protein suggest that HuR may be regulated at the level of its biosynthesis and that the protein follows the fate of its target mRNAs as dictated by downstream associations with RNPs and microRNAs. This possibility remains to be explored.

Irrespective of the regulation of HuR, its protective effects against inflammation and cancer are of imminent biomedical significance. The exploitation of HuR as a therapeutic target has started to gain interest but is based solely on its consideration as an mRNA stabilizer, supporting the identification of compounds that can block binding of HuR to its targets (52). This approach is put into question by our data suggesting that, at least for inflammatory responses, strategies aimed at enhancing HuR activity and biasing its functions toward suppression are of high clinical value against pathologic inflammation and cancer.

Methods

Mice. The *Elavl1*$^{fl/fl}$ strain was derived from the strain reported in ref. 24, following germline excision of a floxed *neo* marker. The 2 lines behaved similarly based on comparisons of data presented in refs. 24 and 25. *LysMCre* mice (26) were provided by Irmgard Forster (University of Munich, Munich, Germany). Lines were maintained in a mixed C57BL/6J, 129Ola background (used for endotoxemia only) or backcrossed to a C57BL/6J background for more than 12 generations (used in all assays). *Tg632*$^{+}$ mice (19) were backcrossed for at least 5 generations to C57BL/6J. To induce HA-HuR, *Tg632*$^{+}$ mice were fed ad libitum with a diet containing 625 mg Dox per kilogram of food (Altromin Spezialfutter GmbH). All mice were bred and maintained in the animal facilities of the Biomedical Sciences Research Center (BSRC) "Alexander Fleming" under specific pathogen–free conditions.

Animal models of acute inflammation and tumorigenesis. For endotoxemia, 10- to 12-week-old mice were injected i.p. with LPS (*Salmonella enteritidis*; Sigma-Aldrich; catalog no. L-6011) at the concentrations indicated in the figures. For measurement of inflammatory mediators, mice were injected i.p. with LPS at 100 μg/25 g body weight. Sera were collected 90 minutes later by cardiac puncture and used for ELISA. For aseptic peritonitis, mice were injected i.p. with Brewer thioglycollate medium (4%; Becton-Dickinson). At the times indicated in results and figures, mice were sacrificed for collection of peritoneal cavity cells, peripheral blood, and bone marrow to be used for flow cytometry. For experimental colitis, 6- to 8-week-old mice were fed ad libitum for up to 2 cycles with water containing 2% (wt/vol) DSS (MW 40,000 kDa; MP Biomedicals Inc.) for 6 days, with intervals of 15 days on regular water. Mice were monitored for weight loss, diarrhea, and rectal bleeding. Values were used for calculation of DAI (53, 54). For induction of CAC, 6- to 8-week-old mice were injected i.p. with 20 mg/kg DMH (Sigma-Aldrich). After 5 days, 1.5%–2% DSS was provided in drinking water for 6 days, followed by 15 days of regular water. This cycle was repeated twice and mice were sacrificed on week 15 for isolation of colonic tissue. Tumor sizes were measured using an electronic Vernier calliper. All measurements were done in a blinded fashion.

Histological analysis. Dissected and opened colons were mounted onto a solid surface and fixed in formalin and paraffin or snap frozen. At least 3–5 serial sections were stained and used for blind histological assessment by a histopathologist. Colitis was graded as described in refs. 53 and 54, incorporating severity and extent of inflammation, crypt damage, and percentage of organ affected. Tumor grading was based on the degree of dysplasia and epithelial differentiation. Immunohistochemical staining was performed on cryostat sections using rat anti-CD68 (FA-11; Abcam) and biotin-conju-

gated anti-HuR (3A2; Santa Cruz Biotechnologies Inc.). Secondary antibodies were from eBioscience. Nuclei were detected with DAPI.

Organ cultures. Whole colons were opened longitudinally, washed with PBS plus 20 mg/ml gentamicin to remove residual intestinal bacteria, and either used for RNA extraction or cut in 1.5-cm pieces into a 48-well plate containing 500 μl RPMI-1640 per well. Tissues were incubated at 37°C/5% CO_2 for 24 hours, and supernatants were collected for cytokine/chemokine ELISA measurements.

Cell culture and chemotaxis. BMDMs and MEFs were isolated as described previously (19, 24). HA-HuR was induced in *Tg632*$^+$ BMDM by addition of 5 μg/ml Dox (D-9891; Sigma-Aldrich). MEFs were also transfected with a vector expressing HA-HuR (pEBBHuR) or empty plasmid (pEBB) using Altrogen Biosystems MEF transfection reagent. For soluble factors, cells were seeded at 1×10^5 to 5×10^5 cells/well in 24-well plates. For non-soluble factors or RNA analyses, cells were seeded at 1×10^7 cells/10 cm^2 plate. Chemotactic assays were performed in 5-μm Transwell filters (Corning Corp). Briefly, filters were conditioned in RPMI plus 0.1% BSA in the absence or presence of recombinant chemokines (Peprotech), macrophage media, or cells for 4–24 hours. Macrophages (10^5) were added on filters and allowed to migrate for 6 hours at 37°C in 5% CO_2. Filters were washed in PBS, fixed in 10% formalin, stained with hematoxylin, mounted, and counted under high power. Four to 5 high-power fields (HPFs) were counted to determine the average number of cells per HPF.

Flow cytometry and protein analysis. For surface antigens, staining was performed using standard procedures. Antibodies were from BD Biosciences (CD11β, Gr1/Ly6G), eBioscience (F4/80), Abcam (CCR2), and R&D Systems (isotypes). Cells were detected and/or sorted using FACSCantoII and FACSVantage flow cytometers. Data were analyzed using FACSDIVA (V.6; BD Biosciences) and FlowJo (V 7.2.5; TreeStar). For additional cytometry procedures, see the Supplemental Methods. For COX2, cell lysates in RIPA buffer were analyzed on 10% SDS-polyacrylamide gels, blotted onto nitrocellulose, and probed with anti-COX2 (Cayman) and anti-GAPDH (6C5; Ambion). For soluble cytokines and chemokines, culture supernatants or fluids were used in ELISAs for IL-1b, IL-10, IL-12p70, TNF-α, TGF-β1 (eBioscience), IL-6 (BD Biosciences), CCL2, and CCL7 (Peprotech).

RNA and R-IP analysis. Total RNA was extracted from macrophages or tissues using TRI Reagent (MRC). qRT-PCR was performed using SsoFast EVA Green Supermix (Bio-Rad) on a RotorGene 6000 machine (Corbet). Expression was normalized to β2-microglobulin and *Gapdh* mRNAs. Relative expression was calculated as the fold difference compared with control values using Bio-Rad RelQuant. For mRNA turnover, BMDMs were treated with actinomycin D, with or without LPS, as previously described (19, 24). mRNA half-lives were calculated by setting the normalized amount of target mRNA (calculated as $Nt = 2^{Ct\,[GAPDH]\,-\,Ct\,[Target]}$) in unstimulated samples to 100 and extrapolating from the corresponding semi-logarithmic plots of percentages versus time. For analysis of polysome-coupled RNA, cytoplasmic fractions containing monosomes and polysomes were isolated from macrophages as previously described (19, 24). R-IP assays were performed using agarose-conjugated anti-HuR (3A2) or control IgG antibodies (Santa Cruz Biotechnology Inc.), as previously described (19, 24). In all cases, data were derived from at least 3 independent biological replicas. Primer sequences, microarray analyses, and meta-analyses are described in the Supplemental Methods. Microarray data were submitted to the Array Express Archive of the EMBL-EBI (http://www.ebi.ac.uk/arrayexpress/) under the record number E-MEXP-2904. For RNA-EMSA, T7 polymerase–transcribed, ^{32}P-labeled probes were generated from PCR-amplified UTR fragments using Maxiscript (Ambion). Following gel purification, probes were refolded and used at a concentration of 45 nM in binding reactions to GST-HuR and in 50 mM HEPES pH 7.6, 25 mM KCl, 2.5 mM $MgCl_2$, 1 mM DTT, and 4% glycerol. Following incubation at 30°C for 10 minutes, fragments were resolved on 4% acrylamide/bis-acrylamide/5% glycerol gels and visualized on a PhosphorImager device using ImageQuant 5.0 software (Molecular Dynamics).

In vitro RNA decay assay. 3′UTRs were PCR amplified from mouse macrophage RNA extracts, sequenced, and cloned in pCY2 vector (55), which provided a 60-nucleotide polyA tail. UTR fragments were annotated via their murine RNA sequences in ENSEMBL accession numbers and included *Tnf* 3′UTR (nucleotides 1110–1619; ENSMUST00000025263), *Gapdh* 3′UTR (1242–1401; ENSMUST00000118875), *Ccr2* 3′UTR (1259–2999; ENSMUST00000055918), and *Ccl2* 3′UTR (539–813; ENSMUST00000000193). Linearized plasmids were used to produce ^{32}P-labeled and m7G(5′)ppp(5′)G-capped RNA substrates. Labeled RNAs (10 ng) were incubated with 2 μg of cytosolic S100 extracts from BMDMs stimulated with LPS for 90 minutes. Reactions were performed at 37°C for the times indicated in Figure 6D, as described in ref. 55, and in 25 μl of a buffer containing 100 mM KCH_3COOH, 2 mM $Mg(CH_3COOH)_2$, 10 mM Tris-Cl pH 7.6, 2 mM DTT, 10 mM creatine phosphate, 1 μg creatine phosphokinase, 1 mM ATP, 0.4 mM GTP, 0.1 mM spermine, and 4U RNasin. Reactions were terminated with 100 μl of 400 mM NaCl, 25 mM Tris-Cl pH 7.6, 0.1% SDS. Precipitated RNAs were analyzed on 5% polyacrylamide/7 M urea gels. Data were quantified using phosphorimaging.

Lentiviral gene transduction. UTR fragments used in stability assays were subcloned onto a modified pLL3.7 lentiviral vector (Clonetech) devoid of loxP sequence and downstream of the GFP coding region. For 3′UTRΔ reporters, nucleotides at positions 1252–1994 and 539–605 were removed using restriction digests of *Ccr2* and *Ccl2* 3′UTRs, respectively. UTR vectors and packaging plasmids were transfected into 293FT cells using LENTI-Smart system (InVivoGen). Lentivirus-containing supernatants were concentrated using LentiX system and introduced into 3-day differentiating bone marrow cultures for 12–16 hours and at an estimated MOI of 5. After extensive washing, cells were further differentiated to BMDMs for 3 more days and used for treatments and flow cytometry.

Statistics. Unless otherwise indicated, Student's 2-tailed unpaired *t* test was used for statistical analysis. *P* values of 0.05 or less were considered statistically significant. Statistical analyses were performed using SigmaPlot version 10.0.

Study approval. Experiments on live animals were approved by the Hellenic Ministry of Rural Development (Directorate of Veterinary Services) and by the Animal Research and Ethics Committee of the BSRC "Alexander Fleming" in compliance with Federation of European Laboratory Animal Science Associations regulations.

Acknowledgments

We thank S. Grammenoudi for help with flow cytometry and the expression profiling facility of BSRC "Alexander Fleming" and V. Aidinis for help with microarray hybridizations. This work was supported by the Association for International Cancer Research (grant AICR-07-0548), European Commission grants MASTERSWITCH (HEALTH-F2-2008-223404) and INFLACARE (HEALTH-F2-2009-223151), and Hellenic Secretariat for Research and Technology grant PENED2003-770.

Received for publication September 6, 2010, and accepted in revised form November 9, 2011.

Address correspondence to: Dimitris L. Kontoyiannis, Institute of Immunology, BSRC "Alexander Fleming", 34 Al. Fleming Str., 166 72 Vari, Greece. Phone: 0030.210.9654335; Fax: 0030.210.9654955; E-mail: kontoyiannis@fleming.gr.

1. Mosser DM, Edwards JP. Exploring the full spectrum of macrophage activation. *Nat Rev Immunol*. 2008;8(12):958–969.
2. Soehnlein O, Lindbom L. Phagocyte partnership during the onset and resolution of inflammation. *Nat Rev Immunol*. 2010;10(6):427–439.
3. Gordon S, Martinez FO. Alternative activation of macrophages: mechanism and functions. *Immunity*. 2010;32(5):593–604.
4. Grivennikov SI, Greten FR, Karin M. Immunity, inflammation, and cancer. *Cell*. 2010;140(6):883–899.
5. Mantovani A, Allavena P, Sica A, Balkwill F. Cancer-related inflammation. *Nature*. 2008; 454(7203):436–444.
6. Anderson P. Post-transcriptional control of cytokine production. *Nat Immunol*. 2008;9(4):353–359.
7. Anderson P. Post-transcriptional regulons coordinate the initiation and resolution of inflammation. *Nat Rev Immunol*. 2010;10(1):24–35.
8. Gaestel M. MAPKAP kinases - MKs - two's company, three's a crowd. *Nat Rev Mol Cell Biol*. 2006; 7(2):120–130.
9. Ruggiero T, et al. LPS induces KH-type splicing regulatory protein-dependent processing of microRNA-155 precursors in macrophages. *FASEB J*. 2009;23(9):2898–2908.
10. Anderson P, Kedersha N. RNA granules: post-transcriptional and epigenetic modulators of gene expression. *Nat Rev Mol Cell Biol*. 2009;10(6):430–436.
11. Pullmann R Jr, et al. Analysis of turnover and translation regulatory RNA-binding protein expression through binding to cognate mRNAs. *Mol Cell Biol*. 2007;27(18):6265–6278.
12. von RC, Gallouzi IE. Decoding ARE-mediated decay: is microRNA part of the equation? *J Cell Biol*. 2008;181(2):189–194.
13. Katsanou V, Dimitriou M, Kontoyiannis DL. Post-transcriptional regulators in inflammation: exploring new avenues in biological therapeutics. *Ernst Schering Found Symp Proc*. 2006;(4):37–57.
14. Doller A, Pfeilschifter J, Eberhardt W. Signalling pathways regulating nucleo-cytoplasmic shuttling of the mRNA-binding protein HuR. *Cell Signal*. 2008;20(12):2165–2173.
15. Brennan CM, Steitz JA. HuR and mRNA stability. *Cell Mol Life Sci*. 2001;58(2):266–277.
16. Rhee WJ, Ni CW, Zheng Z, Chang K, Jo H, Bao G. HuR regulates the expression of stress-sensitive genes and mediates inflammatory response in human umbilical vein endothelial cells. *Proc Natl Acad Sci U S A*. 2010;107(15):6858–6863.
17. López de Silanes I, Lal A, Gorospe M. HuR: post-transcriptional paths to malignancy. *RNA Biol*. 2005; 2(1):11–13.
18. Galban S, et al. RNA-binding proteins HuR and PTB promote the translation of hypoxia-inducible factor 1alpha. *Mol Cell Biol*. 2008;28(1):93–107.
19. Katsanou V, et al. HuR as a negative post-transcriptional modulator in inflammation. *Mol Cell*. 2005;19(6):777–789.
20. Kawai T, Lal A, Yang X, Galban S, Mazan-Mamczarz K, Gorospe M. Translational control of cytochrome c by RNA-binding proteins TIA-1 and HuR. *Mol Cell Biol*. 2006;26(8):3295–3307.
21. Kuwano Y, et al. MKP-1 mRNA stabilization and translational control by RNA-binding proteins HuR and NF90. *Mol Cell Biol*. 2008;28(14):4562–4575.
22. Meisner NC, Filipowicz W. Properties of the regulatory RNA-binding protein HuR and its role in controlling miRNA repression. *Adv Exp Med Biol*. 2010; 700:106–123.
23. Ghosh M, et al. Essential role of the RNA-binding protein HuR in progenitor cell survival in mice. *J Clin Invest*. 2009;119(12):3530–3543.
24. Katsanou V, et al. The RNA-binding protein Elavl1/HuR is essential for placental branching morphogenesis and embryonic development. *Mol Cell Biol*. 2009;29(10):2762–2776.
25. Papadaki O, Milatos S, Grammenoudi S, Mukherjee N, Keene JD, Kontoyiannis DL. Control of thymic T cell maturation, deletion and egress by the RNA-binding protein HuR. *J Immunol*. 2009; 182(11):6779–6788.
26. Clausen BE, Burkhardt C, Reith W, Renkawitz R, Forster I. Conditional gene targeting in macrophages and granulocytes using LysMcre mice. *Transgenic Res*. 1999;8(4):265–277.
27. Sag D, Carling D, Stout RD, Suttles J. Adenosine 5′-monophosphate-activated protein kinase promotes macrophage polarization to an anti-inflammatory functional phenotype. *J Immunol*. 2008; 181(12):8633–8641.
28. Zhu QY, Liu Q, Chen JX, Lan K, Ge BX. MicroRNA-101 targets MAPK phosphatase-1 to regulate the activation of MAPKs in macrophages. *J Immunol*. 2010;185(12):7435–7442.
29. Terzic J, Grivennikov S, Karin E, Karin M. Inflammation and colon cancer. *Gastroenterology*. 2010; 138(6):2101–2114.
30. Allen IC, et al. The NLRP3 inflammasome functions as a negative regulator of tumorigenesis during colitis-associated cancer. *J Exp Med*. 2010; 207(5):1045–1056.
31. Ishikawa TO, Herschman HR. Tumor formation in a mouse model of colitis-associated colon cancer does not require COX-1 or COX-2 expression. *Carcinogenesis*. 2010;31(4):729–736.
32. Rajasingh J, et al. IL-10-induced TNF-alpha mRNA destabilization is mediated via IL-10 suppression of p38 MAP kinase activation and inhibition of HuR expression. *FASEB J*. 2006;20(12):2112–2114.
33. Fan J, et al. Chemokine transcripts as targets of the RNA-binding protein HuR in human airway epithelium. *J Immunol*. 2011;186(4):2482–2494.
34. Mantovani A, Sica A, Sozzani S, Allavena P, Vecchi A, Locati M. The chemokine system in diverse forms of macrophage activation and polarization. *Trends Immunol*. 2004;25(12):677–686.
35. Xu L, et al. Regulation of CCR2 chemokine receptor mRNA stability. *J Leukoc Biol*. 1997;62(5):653–660.
36. Mantovani A, Sica A, Locati M. Macrophage polarization comes of age. *Immunity*. 2005;23(4):344–346.
37. Lim SJ, Lee SH, Joo SH, Song JY, Choi SI. Cytoplasmic expression of HuR is related to cyclooxygenase-2 expression in colon cancer. *Cancer Res Treat*. 2009; 41(2):87–92.
38. Young LE, Sanduja S, Bemis-Standoli K, Pena EA, Price RL, Dixon DA. The mRNA binding proteins HuR and tristetraprolin regulate cyclooxygenase 2 expression during colon carcinogenesis. *Gastroenterology*. 2009;136(5):1669–1679.
39. Brosens LA, et al. Increased expression of cytoplasmic HuR in familial adenomatous polyposis. *Cancer Biol Ther*. 2008;7(3):424–427.
40. Geissmann F, Jung S, Littman DR. Blood monocytes consist of two principal subsets with distinct migratory properties. *Immunity*. 2003;19(1):71–82.
41. Deshmane SL, Kremlev S, Amini S, Sawaya BE. Monocyte chemoattractant protein-1 (MCP-1): an overview. *J Interferon Cytokine Res*. 2009;29(6):313–326.
42. Gunn MD, Nelken NA, Liao X, Williams LT. Monocyte chemoattractant protein-1 is sufficient for the chemotaxis of monocytes and lymphocytes in transgenic mice but requires an additional stimulus for inflammatory activation. *J Immunol*. 1997; 158(1):376–383.
43. Winter C, et al. Lung-specific overexpression of CC chemokine ligand (CCL) 2 enhances the host defense to Streptococcus pneumoniae infection in mice: role of the CCL2-CCR2 axis. *J Immunol*. 2007; 178(9):5828–5838.
44. Motomura Y, et al. Induction of a fibrogenic response in mouse colon by overexpression of monocyte chemoattractant protein 1. *Gut*. 2006; 55(5):662–670.
45. Khan WI, et al. Critical role of MCP-1 in the pathogenesis of experimental colitis in the context of immune and enterochromaffin cells. *Am J Physiol Gastrointest Liver Physiol*. 2006;291(5):G803–G811.
46. Popivanova BK, et al. Blockade of a chemokine, CCL2, reduces chronic colitis-associated carcinogenesis in mice. *Cancer Res*. 2009;69(19):7884–7892.
47. Tokuyama H, et al. The simultaneous blockade of chemokine receptors CCR2, CCR5 and CXCR3 by a non-peptide chemokine receptor antagonist protects mice from dextran sodium sulfate-mediated colitis. *Int Immunol*. 2005;17(8):1023–1034.
48. Penton-Rol G, et al. Selective inhibition of expression of the chemokine receptor CCR2 in human monocytes by IFN-gamma. *J Immunol*. 1998; 160(8):3869–3873.
49. Sica A, et al. Bacterial lipopolysaccharide rapidly inhibits expression of C-C chemokine receptors in human monocytes. *J Exp Med*. 1997;185(5):969–974.
50. Mukherjee N, et al. Integrative regulatory mapping indicates that the RNA-binding protein HuR couples pre-mRNA processing and mRNA stability. *Mol Cell*. 2011;43(3):327–339.
51. Keene JD. RNA regulons: coordination of post-transcriptional events. *Nat Rev Genet*. 2007;8(7):533–543.
52. Meisner NC, et al. Identification and mechanistic characterization of low-molecular-weight inhibitors for HuR. *Nat Chem Biol*. 2007;3(8):508–515.
53. Maines LW, et al. Suppression of ulcerative colitis in mice by orally available inhibitors of sphingosine kinase. *Dig Dis Sci*. 2008;53(4):997–1012.
54. Wirtz S, Neufert C, Weigmann B, Neurath MF. Chemically induced mouse models of intestinal inflammation. *Nat Protoc*. 2007;2(3):541–546.
55. Chen CY, et al. AU binding proteins recruit the exosome to degrade ARE-containing mRNAs. *Cell*. 2001;107(4):451–464.